



Numerical analysis of mono and hybrid nanofluids-cooled micro finned heat sink for electronics cooling-(Part-I)

Adeel Arshad^{a,b,*}, Muhammad Ikhlaz^{c,d}, Muhammad Saeed^e, Muhammad Imran^b

^a Environment and Sustainability Institute (ESI), Faculty of Environment, Science and Economy, University of Exeter, Penryn Campus, Cornwall TR10 9FE, United Kingdom

^b Department of Mechanical, Biomedical and Design Engineering, Aston University, Birmingham B4 7ET, United Kingdom

^c School of Engineering, Newcastle University, Newcastle Upon Tyne NE1 7RU, United Kingdom

^d The Dyson Institute of Engineering and Technology, Malmesbury SN16 0RP, United Kingdom

^e Abu Dhabi Maritime Academy, P.O. Box 54477, Abu Dhabi, United Arab Emirates

ARTICLE INFO

Keywords:

Thermohydraulic performance
Nanofluid
Micro pin-fin
Heat sink
Heat and fluid flow

ABSTRACT

This study explores the thermohydraulic performance of metallic-oxide and carbon-additives-based mono and hybrid nanofluids-cooled micro pin-fin heat sink by adopting the multiphase Eulerian model. The circular configuration is adopted for micro pin-fins, with the staggered arrangement and constant heat flux applied at the base of the heat sink. The mono and hybrid nanofluids are based on an aqueous solution of Ag, MgO, GNP, MWCNT, Ag-MgO, and GNP-MWCNT mono and hybrid nanoparticles, and a pressure drop (Δp) range is applied across the heat sink. The heat transfer and fluid flow performance are evaluated in terms of temperature difference (ΔT), thermal resistance (R_{th}) of the heat sink, average heat transfer coefficient (h_{avg}), average Nusselt number (Nu_{avg}), pumping power (PP), overall performance (OP), and performance evaluation criteria (PEC), whereas the velocity, temperature, pressure coefficient, and flow streamline contours present the qualitative depiction of flow distributions across the heat sink. The results revealed that under certain Δp conditions, the GNP dispersed mono nanofluid showed the highest thermal performance of the micro pin-fin heat sink compared to the water as a coolant. The optimal nanoparticle loading (ϕ) is found between 0.50 % and 0.75 % of GNP nanoparticles. The maximum enhancement in PEC is achieved at 60 % for ϕ of 0.50 % and 0.75 % for both Δp of 1120 Pa and 1470 Pa, respectively. At an optimum Δp , the higher average h_{avg} , Nu_{avg} , and lower R_{th} are achieved.

1. Introduction

The rapid advancement of the electronics industry is increasingly challenged by overheating issues, particularly due to the compactness of modern circuitry. This miniaturization trend leads to higher heat generation within limited spaces, posing significant challenges to thermal management. Data centres, a critical component of the global digital infrastructure, consume approximately 1.31 % of global electricity, with a substantial 33 % dedicated to cooling systems [1]. The operational reliability of integrated circuits (ICs) is notably affected by temperature, as a mere 2 °C increase can reduce their reliability by 10 %. Overheating is a major cause of electronic component failure, accounting for 55 % of such incidents, while other factors like vibration, humidity, and dust contribute to the remaining 45 % [2]. Traditional cooling methods often struggle to meet advanced thermal management demands, partly due to

the use of coolants with inherently low thermal conductivity. Additionally, the effectiveness of these cooling methods is influenced by the geometric configuration and operating parameters.

In response, a variety of innovative cooling strategies have been explored in recent research. These include optimizing heat sink geometry [3,4] employing advanced coolants such as metal-based nanofluids [5–7], carbon-additives based nanofluids [8,9], supercritical CO₂ [10, 11], and hybrid nanofluids [12,13]. These approaches are driven by the need for cooling technologies that offer superior thermal conductivity and convective heat transfer rates to keep pace with the demanding thermal requirements of high-tech electronics. Nanofluids, particularly those combining metal or carbon nanoparticles with conventional fluids, demonstrate enhanced thermal properties. These fluids boast a high surface-to-volume ratio and an increased solid-liquid interface, which can lead to improved interphase heat exchange [14,15]. However, it is important to note that achieving excellent suspension stability remains a

* Corresponding author.

E-mail address: a.arshad@exeter.ac.uk (A. Arshad).

Nomenclature	
<i>Abbreviations</i>	
GNP	graphene nanoplatelet
MWCNT	multi walled carbon nanotube
MgO	magnesium oxide
Ag	silver
OP	overall performance
PEC	performance evaluation criteria
<i>Symbols</i>	
C_D	drag force
d_{fin}	fin diameter (m)
d_h	hydraulic diameter (m)
D_p	particle diameter (m)
D	diameter of the inlet and outlet port (m)
f_d	drag function
h_{avg}	convective heat transfer coefficient (W/m ² .K)
h_{fin}	fin height (m)
H_{HS}	height of the Heat Sink
\dot{H}	heat flux (W/m ²)
k	thermal conductivity (W/m.K)
L_{HS}	length of the heat sink (mm)
l_h	length of the Finned area (m)
Nu	Nusselt number
PP	pumping Power (W)
\dot{Q}	input Power (W)
Δp	pressure drop (Pa)
\dot{q}	heating input (kW/m ²)
Q	volumetric flow rate (m ³ /s)
R_{th}	thermal Resistance (K/W)
Re_p	particle Reynolds number
T	temperature (°C)
V_{kmv} , V_{pm}	drift velocity (m/s)
$V_{relative}$	relative/Slip velocity (m/s)
W_{HS}	width of the heat sink
w_h	width of the finned area (m)
<i>Greek symbols</i>	
ρ	density (kg/m ³)
φ	volume fraction of nanoparticles
μ	viscosity (N.s/m ²)
τ_m	shear stress tensor
<i>Sub/super scripts</i>	
c	continuous phase
d	drift
f	fin
k	specie
m	mean
p	particle phase

significant challenge in many applications of nanofluids, potentially limiting their effectiveness. Recent advancements in heat sink technology focus on the use of pin-fins and nanofluids for enhanced cooling. The below review presents a detailed analysis of recent studies, each offering unique insights into heat sink design and optimization.

Yan et al. [16] employed numerical simulations to analyze alumina/water nanofluid flow in heat sinks with pin-fins. Key findings include the reduction of maximum and average heat sink temperatures with increased Reynolds number, lower outlet temperature, and higher pressure drop. Square pin-fins were found to generate more entropy compared to rhombic pin-fins. Dey et al. [13] focused on the cooling performance of Highly Concentrating Photovoltaic/Thermal (HCPV/T) systems using nanofluids and pin-finned heat sinks. Significant temperature reduction in solar cells was achieved using MWCNT nanofluid, with staggered arrangements of pin-fins showing higher heat transfer characteristics. The study highlighted the influence of MWCNT volume concentration and pin-fin arrangements on thermal performance. Ambreen et al. [17] conducted a numerical research by employing the circular pin-fin heat sink with Al₂O₃ dispersed aqueous nanofluid with volume fraction from 0 % to 1 % as a coolant. They studied the heat and flow dynamics of nanofluid at varying operating conditions for cooling of for the purpose of thermal management. Their study concluded that with the addition of Al₂O₃ into water demonstrated an enhancement of 16 % in average heat transfer coefficient. In another study [18], they explored the effects of hybrid nanoparticles of Cu and Al₂O₃ into water with volume of 1 % flowing through the diamond, circular and elliptical configured pin-fin heat sinks. They found that average Nusselt number was enhanced of 19.65 %, 24 %, and 25.14 % for circular, elliptical, and diamond fins, respectively. Shahsavari et al. [19] studied the fluid position of a single-phase flow at inlet and outlet of a micro pin-fin heat sink numerically at Reynolds number range of 500 to 2000. They found that input and output at opposite side along the longitudinal length gave the higher performance evaluation criteria value of 1.131. Similarly, Shahsavari et al. [20] numerically investigated the effect of perforation angle of perforated pin-fin heat sink under single-phase flow at various Reynolds numbers of 500–2000. They found the highest performance

evaluation criteria of 11.06 % to 16.63 % with perforation angle of 45° compared to the 0° Wang and Hai [21] conducted research on optimizing the performance of pin-fin heat sinks with splitters, using water and water-Al₂O₃ nanofluids as coolants. Their study focused on improving the hydrothermal performance of heat sinks, which is essential for cooling CPU systems. The introduction of splitters increased the heat transfer surface area and improved fluid mixing, leading to enhanced heat transfer efficiency. Furthermore, the use of nanofluids boosted thermal conductivity, contributing to more effective heat dissipation. These modifications resulted in a significant reduction in CPU temperatures, thereby improving the overall performance of the cooling system.

In another study, Shahsvar et al. [22] conducted an investigation on analyzing thermal and frictional irreversibility in heatsinks and the use of splitters in heat sinks, but with variations in coolant types or heat sink configurations. They highlighted different aspects of splitter technology, focusing on different operational conditions or electronic devices, offering a broader perspective on the application of this technology. Their methodology included a combination of computational fluid dynamics simulations and experimental tests, similar to Wang and Hai [21], but with a focus on different performance metrics such as pressure drop and flow turbulence. Both studies underscored the value of splitters in enhancing heat transfer efficiencies. However, differences emerged in terms of the types of coolants used, the specific applications targeted, and the detailed outcomes related to thermal and fluid dynamics. For example, Shahsvar et al. used synthetic coolants targeting applications like automotive cooling systems, in contrast to Wang and Hai's use of water-based nanofluids for CPU cooling. Ahsaee et al. [23] investigated the effect of ultrasound waves on pin-fin heat sinks, revealing that certain configurations can significantly reduce thermal entropy generation while increasing frictional entropy generation. In another study, Ahsaee et al. [24] investigated the effect of inlet velocity profiles on a pin-fin heat sink. Results indicated that non-uniform velocity profiles offer better hydrothermal performance and lower frictional entropy generation compared to uniform profiles.

Zhu et al. [25] designed and simulated a circular heat sink with

cylindrical pin-fins, studying the effects of pin-fin dimensions and inlet velocity profiles on heat transfer characteristics. Haque et al. [26] conducted a numerical analysis of water/silver nanofluid flow in a perforated pin-fin heat sink, focusing on the impact of perforation inclination angles on heat transfer and entropy generation. Haghghi et al. [27] carried out an experimental investigation exploring the forced convection heat transfer performance of different Plate Pin-Fin Heat Sink (PPFHS) models with varying fin-pin spacing using air as the coolant. The study found that optimal fin-pin spacing enhances heat transfer efficiency and airflow management, with empirical correlations developed to predict performance. Heatsinks with conical pins and 7-fin configurations exhibited the best thermal performance. These findings are crucial for designing efficient PPFHS heatsinks, emphasizing the importance of fin-pin spacing in thermal management systems. Wang et al. [28] conducted an experimental investigation comparing forced convection heat transfer across different heat sink models, identifying optimal fin-pin spacing and heat sink configurations. Liu et al. [29] investigated flow and heat transfer of nanofluid in pin-fin heat sinks, assessing the impact of Reynolds number, nanoparticle concentration, and splitters on entropy generation and heat dissipation. Harris et al. [30] conducted a numerical analysis of biomorphic pin-fin heat sinks and studied the heat transfer and flow characteristics under Reynolds number 5500–13,500. They found that plain hexagon top design pin-fin revealed the higher heat transfer coefficient and Nusselt number. This novel design enhanced the heat transfer performance 1.5 to 1.7 times compared to the rectangular and square fin designs.

The reviewed studies collectively enhance the understanding of heat sink design and optimization. The reviewed studies can be categorized based on the type of coolant used, heat sink geometry, and optimization methods as listed in Table 1. Studies using water/synthetic coolants, such as those by Shahsavari et al. [22], found that arched splitters minimize entropy generation. Research utilizing silver/water nanofluids, like that by Shahsavari et al. [22] and Ghazizade-Ahsaei et al. [24], revealed that perforations and varying inlet velocities can improve heat transfer. Studies with nanofluids, including work by Dey et al. [13], Haque et al. [26], and Wang et al. [28], demonstrated enhanced cooling performance with different geometries, such as pin fins and elliptical fins. Hai et al.'s [31] research on Fe₃O₄ ferrofluid showed that magnetic fields can further improve cooling efficiency. In terms of geometry, pin fin designs were widely used and optimized across several studies, while

elliptical and circular fins, explored by Haque et al. [26] and Zhu et al. [25] respectively, offered high thermal performance. Optimization methods varied, with numerical techniques used in most studies, showing significant improvements in thermal efficiency. AI-based approaches, highlighted by Yan et al. [16], Zhu et al. [25], and Liu et al. [29], were particularly effective in reducing maximum temperatures and identifying key factors influencing thermal efficiency. Overall, both numerical and AI-based optimization methods have proven to significantly enhance heatsink performance. Following points were deduced from the above-mentioned studies.

Key insights include.

- Reynolds Number and Flow Rate: Higher Reynolds numbers and flow rates generally lead to lower heat sink temperatures but increase pressure drops.
- Pin-Fin Geometry: Square pin-fins often generate more entropy than rhombic pin-fins, and specific shapes like elliptical pin-fins can significantly enhance hydro-thermal performance.
- Nanofluids and Magnetic Fields: The use of nanofluids, particularly MWCNT and alumina/water, significantly improves cooling performance. Magnetic fields further enhance this effect, especially in microchannel heat sinks with ferrofluid.
- Inlet Velocity Profiles: Non-uniform velocity profiles yield better hydrothermal performance and lower frictional entropy generation compared to uniform profiles.
- Ultrasound Waves and Splitters: The application of ultrasound waves and the use of splitters in heat sinks can optimize heat transfer and reduce entropy generation.

Hence the literature review demonstrates the effectiveness of various strategies in enhancing heat sink performance. Future research should continue exploring innovative materials, geometries, and external influences like magnetic fields and ultrasound waves to further improve cooling systems in diverse applications. However, the use of nanofluids, especially hybrid variants, in conjunction with micro pin-fin heat sinks has been explored by only a few researchers [32–34]. In this context, the current study delves into the thermohydraulic performance of mono and hybrid nanofluids in an aqueous solution, circulating through a micro pin-fin heat sink with a circular configuration. It focuses on various pressure drop (Δp) ranges, employing a multiphase Eulerian model for

Table 1
Summary of key studies on heatsink optimization based on coolant, geometry, and method of analysis.

Study	Scope	Coolant	Geometry	Method of Analysis	Main Conclusion
Dey et al. [13]	Thermal analysis of pin-finned heatsinks in HCPV/T systems	MWCNT/Water nanofluid	Pin-Fin	Numerical	Nanofluids and pin-fins enhance cooling performance
Yan et al. [16]	Optimizing pin-finned heat sink designs using AI and simulations	Al ₂ O ₃ /Water nanofluid	Pin-Fin	Numerical	AI and simulations effectively reduce maximum temperature
Ambreen et al. [17]	Heat and flow analysis of pin-fin heat sink using nanofluid	Al ₂ O ₃ /Water nanofluid	Pin-Fin	Numerical	Nanofluid enhance the average heat transfer coefficient of 16%
Ambreen et al. [18]	Optimizing the pin-fins using hybrid nanofluid	Cu-Al ₂ O ₃ /Water nanofluid	Pin-Fin	Numerical	The highest Nusselt number enhancement of 25.14% with diamond fins
Wang et al. [21]	Optimizing pin-fin micro heat sinks	Water and water/Al ₂ O ₃ nanofluids	Pin-Fin	Numerical	Optimized designs enhance thermal performance
Shahswar et al. [22]	Analyzing thermal and frictional irreversibility in heatsinks	Water/synthetic coolants	Pin-Fin	Numerical	Arched splitters show the lowest entropy generation
Shahsavari et al. [20]	Analyzing the effect of perforations in heatsinks	Water/Ag nanofluid	Perforated Pin-Fin	Numerical	Perforations improve heat transfer
Ghazizade-Ahsaei et al. [24]	Impact of inlet velocity on entropy generation in heatsinks	Water/Ag nanofluid	Pin-Fin	Numerical	Similar heat transfer coefficients across different profiles
Zhu et al. [25]	Optimizing circular heatsink designs with cylindrical pins using AI	Al ₂ O ₃ /Water nanofluid	Circular Fin	AI-based	Enhanced cooling performance with AI optimization
Haque et al. [26]	Examining elliptical-shaped pin fins in heatsinks	Nanofluids	Elliptical Fin	Numerical	Elliptical pin fins offer high thermal performance
Wang et al. [28]	Optimizing nanofluid flow in heatsinks	Nanofluid	Pin-Fin	Numerical	Optimization reduces entropy, enhancing efficiency
Liu et al. [29]	AI analysis of entropy generation in nanofluid flows	Al ₂ O ₃ /Water nanofluid	Various, including pin-fin	AI-based	AI helps identify key factors affecting entropy generation

numerical analysis with a constant and varying volume fraction. It also provides valuable insights into the design and optimization of heat sink systems, highlighting the potential of various pin-fin configurations and nanofluids to enhance cooling efficiency in modern electronic applications.

2. Problem description and numerical formulation

An aluminum-made and circular geometry of micro pin-fins heat sink with the staggered arrangement was modelled, as shown in Fig. 1. A constant heat flux (\dot{q}) of 300 kW/m² was applied at circular micro pin-fins (CMPFs) heat sink base and Δp was varied in the range of 570 Pa \leq $\Delta p \leq$ 2760 Pa. The detailed dimensions of used CMPFs heat sink are mentioned in Table 2. The mono and hybrid nanoparticles of Ag, MgO, GNP, MWCNT, Ag-MgO, and GNP-MWCNT of volume fraction (φ) of 1.0 % were considered with water and later varying φ of 0 %, 0.25 %, 0.50 %, 0.75 %, and 1.0 % of GNP nanoparticles were further investigated as mono nanofluid. The multiphase Eulerian approach is considered under laminar, steady-state, and incompressible flow conditions. The continuity, momentum, and energy equations for p^{th} phases and mixture quantities are defined as follows:

Mixture continuity:

$$\nabla \cdot (\rho_m \vec{V}_m) = 0 \quad (1)$$

Mixture conservation of momentum:

$$\nabla \cdot (\rho_m \vec{V}_m \vec{V}_m) = -\nabla P_m + \nabla \cdot \tau_m + \rho_m \mathbf{g} - \nabla \cdot \sum_{k=1}^2 \varphi_k \rho_k \vec{V}_{km} \vec{V}_{km} \quad (2)$$

The shear stress tensor, velocity, and volume fraction in the above equation are denoted by τ_m , \vec{V}_m , and α respectively. \vec{V}_{km} is the drift velocity and can be estimated using the Eq. (3).

$$\vec{V}_{km} = \vec{V}_k - \vec{V}_m \quad (3)$$

The drift velocity can then be utilized to estimate the mixture velocity and density using Eqs. (4) and (5), respectively.

$$\vec{V}_m = \frac{\sum_{k=1}^2 \varphi_k \rho_k \vec{V}_{km}}{\rho_m} \quad (4)$$

$$\rho_m = \sum_{k=1}^2 \varphi_k \rho_k \quad (5)$$

The relative/slip velocity can relate to drift velocity using Eq. (6), this equation is valid for the flow field of a two-component fluid but can be extended for the higher number phases.

Table 2
Dimensions of CMPFs heat sink.

Parameter	Dimension (mm)
L_{HS}	21
W_{HS}	18
H_{HS}	4
l_h	10
w_h	10
h_{fm}	2.5
d_{fm}	0.66
$D_m = D_{out}$	2

$$\vec{V}_{pm} = V_{relative} = \frac{\varphi_p \rho_p}{\rho_m} V_{relative} = \frac{\varphi_c \rho_c}{\rho_m} V_{relative} \quad (6)$$

α_c and ρ_c are the volume fraction and fluid density for the continuous phase or the primary phase which is water in the present case. To complete the mixture model, constitutive equations are needed, and then the slip velocity can be obtained with the help of an algebraic equation defined by Manninen et al. [35].

$$V_{relative} = \frac{\rho_p d_p^2}{18 \mu_d f_d} \left(\frac{\rho_p - \rho_m}{\rho_p} \right) \left[\mathbf{g} - (\vec{V}_m \cdot \nabla) \vec{V}_m - \frac{\partial \vec{V}_m}{\partial t} \right] \quad (7)$$

The drag coefficient (C_D) can be utilized to evaluate the drag function (in Eq. (7)) using Eq. (8) [36]. The particle-particle interaction is neglected in the study which is why the agglomeration and collision of nanoparticles is not considered. These interactions are important when conducting the molecular dynamics simulation [37,38].

$$f_d = C_D \frac{Re_p}{24} = 1 + 0.15 Re_p^{0.687} \quad Re_p \leq 1000 \quad (8)$$

Mixture conservation of energy:

Eq. (9) presents the energy conservation equation of the mixture.

$$\nabla \cdot (\rho_m \vec{V}_m \dot{H}_m) = -\nabla \cdot (q_m) - \nabla \cdot \sum_{k=1}^2 \varphi_k \rho_k \vec{V}_{km} \dot{H}_k \quad (9)$$

The heat flux due to conduction and the mixture enthalpy are denoted by q_m and H_m . The volume fraction equation can be used to estimate the particle distribution in the primary phase, the continuity derived for the particle phase using a constant density method can be used as mentioned in Eq. (10).

$$\nabla \cdot (\varphi_p \vec{V}_m) = -\nabla \cdot (\varphi_p \vec{V}_{pm}) \quad (10)$$

The relative velocity between fluid phase and particle phase can be

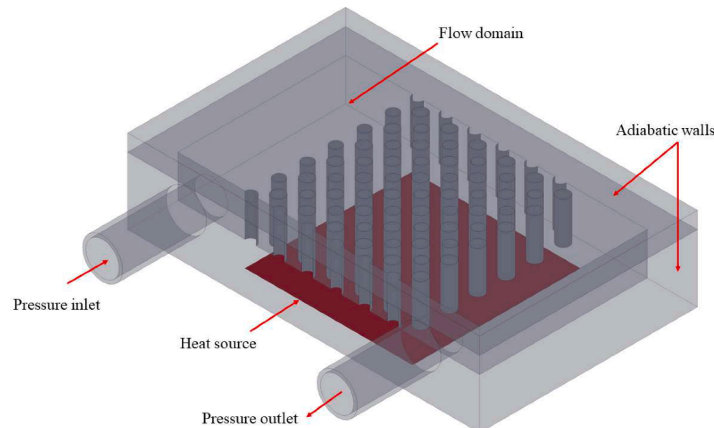


Fig. 1. Schematic heat sink with boundary conditions.

used to calculate the particle Reynolds number $\left(Re_p = \frac{d_p \rho_c V_{relative}}{\mu_c}\right)$, the fluid density, particle diameter and viscosity are denoted by ρ_c , d_p , and μ_c , respectively.

The thermophysical properties of the base fluid and nanoparticles used in the current study are listed in Table 3.

Steady-state 3D Eulerian-Eulerian multiphase simulations were conducted, the schematic diagram of the computational domain is shown in Fig. 1 [37,38]. The present conjugate heat transfer problem has been simulated using the Finite Volume Method (FVM) by utilizing commercial software (Ansys-FLUENT). The coupling of pressure and velocity has been estimated using the coupled scheme. The pressure terms have been discretized using the standard scheme, while the interpolation of the remaining parameters has been carried out using the second-order upwind scheme. The total mass of the injected particles (secondary phase) has been calculated considering the Reynolds number, viscosity, density, and nanoparticle volume fraction of the nanofluid. The velocity and temperature of the nanoparticles are assumed to be equivalent to the base fluid. To reduce the maximum mass residuals of the grid control volume, the convergence criteria for all parameters (continuity, momentum, energy) have been restricted to 10^{-05} [40]. The heat sink base is exposed to constant heat flux, the pressure inlet boundary condition is applied at the inlet of the heat sink, and the pressure outlet is defined at the outlet of the heat sink. All walls, except for the interfaces, have been treated as adiabatic, and a no-slip boundary condition has been imposed. The inlet fluid temperature is considered as the ambient temperature, and the outlet pressure is considered as the ambient pressure. The escape boundary condition has been implemented for the discrete phase at the heat sink inlet and outlet, while the walls of the heat sink have been assigned the reflect boundary condition.

The average Nusselt number (Nu_{avg}), the surface heat transfer coefficient (h_s), heat sink pumping power (PP), thermal resistance (R_{th}), volumetric flow rate (Q), overall heat sink performance (OP) and Performance Evaluation Criterion (PEC) are estimated by Eq. (11) to Eq. (16), respectively [30,42].

$$Nu_{avg} = \frac{h_{avg} d_h}{k_{nf}} \quad (11)$$

$$h_s = \frac{\dot{q}}{T_s - T_f} \quad (12)$$

$$R_{th} = \frac{T_b - T_{in}}{\dot{q}} \quad (13)$$

$$PP = Q \times \Delta p \quad (14)$$

$$OP = \frac{\dot{Q}}{PP} \quad (15)$$

Table 3
Thermophysical properties of base fluid and nanoparticles [20,39–41].

Material	ρ (kg/m ³)	k (W/m.K)	μ (kg/m.s)	c_p (J/kg.K)	Size	M. W (g/mol)
H ₂ O	997.1	0.613	0.00103	4179	–	18.015
Al	2719	202.37	–	871.0	–	26.981
Ag	10,500	429	–	235	$d = 100$ nm	107.87
MgO	3580	61.923	–	921	$d = 35$ nm	40.3
GNP	2200	3000	–	790	$t = 3-5$ nm $d < 10$ μ m	12.01
MWCNT	2100	1500	–	630	$d = 6-13$ nm $l = 2.5-20$ μ m	12.01

$$PEC = \frac{Nu_{nf}/Nu_t}{\Delta p_{nf}/\Delta p_t} \quad (16)$$

Where, Δp and Q represent the pressure drop across the test section and volumetric flow rate, respectively.

A grid convergence study is conducted before obtaining any results and validated by utilising a Grid Convergence Index (GCI) method [43]. Later, results were validated against the single-phase benchmark numerical [17] and experimental data [44], as shown in Fig. 2. It can be seen that the flow rate across the pressure drop gives quite accurate values, but some deviation can be observed for the thermal resistance of the heat sink with respect to the pressure drop but still with an acceptable limit. The trend quite matches that thermal resistance decreases with an increase in pressure drop.

3. Results and discussion

This section discusses the results of CMPFs heat sink cooled with mono and hybrid nanofluids based on metallic-oxide and carbon additives nanoparticles under different Δp across the inlet and outlet. Fig. 3a represents the variations of thermal resistance (R_{th}) in case of water and nanofluids under different Δp conditions as result of augmented flow velocity. A decreasing trend in R_{th} is observed with the increase of Δp for all flowing fluids through the heat sink which means a uniform heat transfer occurs along with mild heat sink temperature. The higher decrease in R_{th} is obtained in case of mono Ag and GNP nanoparticles dispersed nanofluids in comparison of their respective hybrid nanoparticles (i.e., Ag-MgO or GNP-MWCNT) based nanofluids. Along with that, Fig. 3a shows the carbon additives (GNP, MWCNT and GNP-MWCNT) dispersed mono and hybrid nanofluids have lower R_{th} in comparison to metallic-oxide (Ag, MgO and Ag-MgO) dispersed nanofluids because of higher thermal conductivity of carbon additives. The decrease in the case of Ag and GNP nanoparticles dispersed mono nanofluids in R_{th} is 25.20 % and 40.71 %, respectively, at Δp of 570 Pa compared to the water-cooled CMPFs heat sink. Similarly, a decrease of 30.74 % and 44.26 % in R_{th} is obtained in case the of Ag and GNP nanoparticles dispersed mono nanofluids at Δp of 2760 Pa compared to the water-cooled CMPFs heat sink which is because of increasing fluid velocity.

Contrarily to the R_{th} , an increasing trend was obtained in average Nusselt number (Nu_{avg}) with the increase of Δp because of enhanced heat transfer rate at higher flow velocity, shown in Fig. 3b. The higher Nu_{avg} shows that there is a higher heat transfer rate with higher convective heat transfer coefficient with the variation of Δp . The increase in Nu_{avg} is higher in case of GNP dispersed mono nanofluid follow on GNP-MWCNT, MWCNT, Ag, Ag-MgO and MgO dispersed nanofluids. Again, it is revealed that the nanoparticles which exhibit higher thermal conductivity such as GNP, MWCNT, Ag and MgO show the higher Nu_{avg} . The enhancement in Nu_{avg} is achieved of 45.06 % and 54.26 % at Δp of 570 Pa and 2760 Pa, respectively, in case of GNP dispersed mono nanofluid compared to the water cooled CMPFs heat sink. The lesser enhancement in Nu_{avg} is obtained with GNP-MWCNT and followed on MWCNT based hybrid and mono nanofluids, respectively, against each Δp in case of carbon additives nanoparticles. Similarly, in case of Ag, MgO and Ag-MgO based mono and hybrid nanoparticles, the higher increase in Nu_{avg} of 15.62 % and 24.23 % is obtained at Δp of 570 Pa and 2760 Pa, respectively, in case of Ag dispersed mono nanofluid compared to the water cooled CMPFs heat sink. It is revealed from Fig. 3a and b that the combination of hybrid nanoparticles of Ag-MgO and GNP-MWCNT show the higher R_{th} and lower Nu_{avg} of because of the addition of MgO and MWCNT which have the lower thermal conductivity compared to GNP and Ag, keeping a constant volume fraction.

The results of volumetric flow rate (Q) of water, mono, and hybrid nanofluids flowing through the heat sink as a function of Δp is shown in

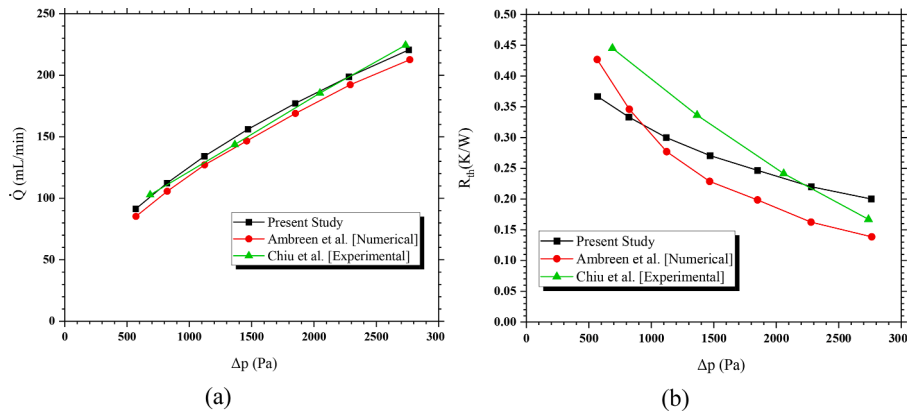


Fig. 2. Validation with experimental and numerical data for different pressure drops across the heat sink, (a) flow rate and (b) thermal resistance.

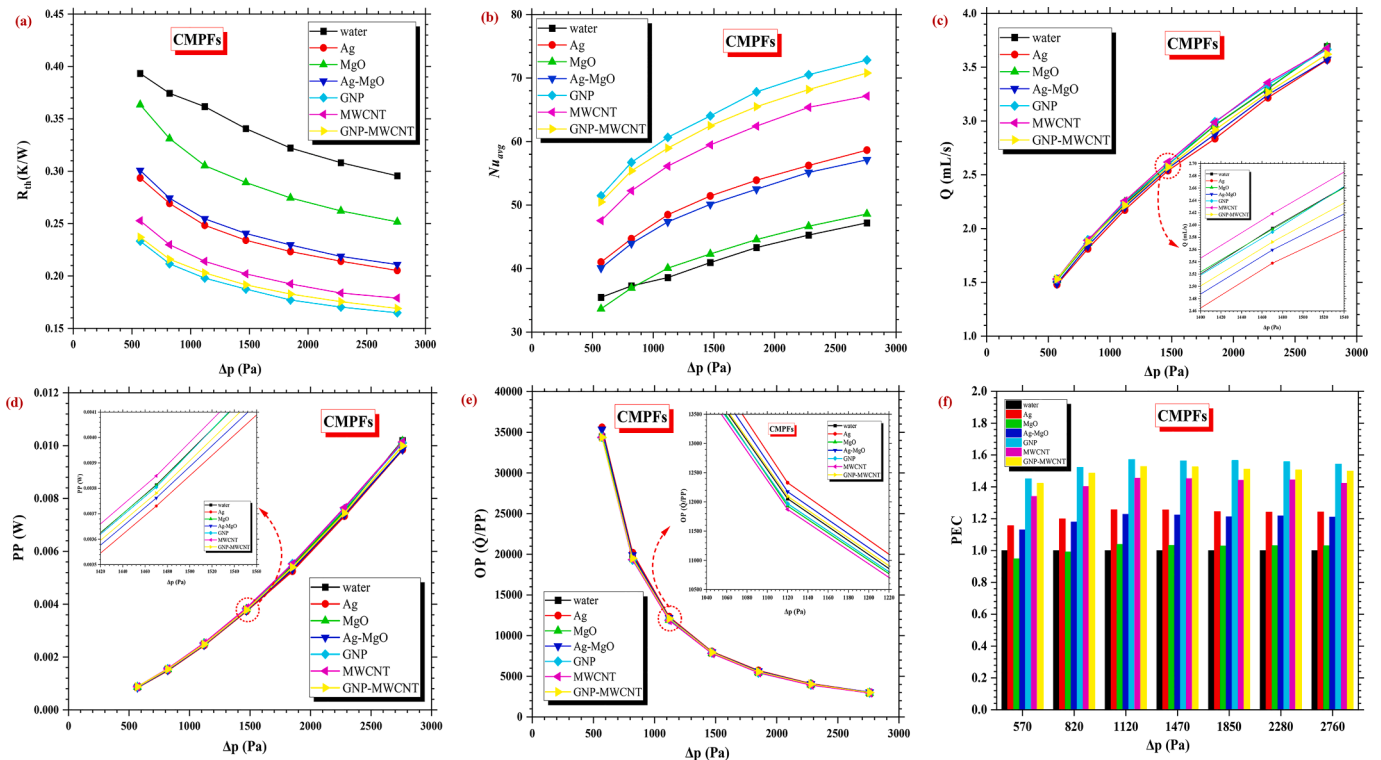


Fig. 3. Variation of (a) R_{th} , (b) Nu_{avg} , (c) Q , (d) PP , (e) OP , and (f) PEC with water, mono and hybrid nanofluids cooled CMPFs heat sink.

Fig. 3c. The higher Q is achieved with the increase of Δp because of the increase in velocity which reveals the same trend reported experimental studies [44]. At lower Δp , there is no significant variation in Q for both in mono and hybrid nanofluids cases flowing through the CMPFs heat sink. The maximum decrease of 2 % in case of Ag nanoparticles dispersed mono nanofluid compared to the water-cooled heat sink. The slight variation in Q of nanofluids is because of highly fluid viscosity which causes the higher flow resistance and slight shear thickening effects by the suspension of nanoparticles.

The similar increasing trend in pumping power (PP) as a function of Δp in cases of all mono and hybrid nanofluids. The dispersion of nanoparticles increases the viscosity of nanofluids which is associated with the shear thickening effect. The slight variation of 1.87 % at $\Delta p = 1470$ Pa is obtained in case of MWCNT dispersed mono nanofluids in comparison with water cooled heat sink. The amplified viscosity of nanofluids certainly requires higher pumping power to achieve the higher flow velocity for enhanced heat transfer rate resulting in a higher cost.

The overall performance (OP) of CMPFs heat sink cooled with water, mono, and hybrid nanofluids is represented in Fig. 3d. The OP is evaluated based on supplied input power (\dot{Q}) and required pumping power (PP) to circular the coolant, which act simultaneously to draw the comprehensive performance of heat sink under different coolants. Since, the OP parameter considers both parameters because it is the ratio of heat transfer to PP . It is revealed that there is no significant difference observed in OP comparing all mono and hybrid nanofluids, as shown in Fig. 3e. The decrease in OP with the increase of Δp is observed because of the increase of PP , as shown in Fig. 3d. The slight variation in OP of 1.95 % is achieved in case of Ag dispersed nanoparticles which is because of individual thermophysical properties since the volume fraction of both mono and hybrid nanoparticles is constant. Furthermore, heating power for all case is constant, therefore the OP is higher at lower Δp or lower fluid flow velocity which requires lower PP . Further, the hydraulic thermal performance of CMPFs heat sink cooled with mono and hybrid nanofluids is analyzed using performance evaluation criteria

(*PEC*) which is the ratio heat transfer enhancement to pressure drop. The *PEC* simultaneously evaluates the effect of two parameters Nusselt number (positive parameter) and pressure drop (negative parameter). The results of *PEC* as a function of Δp are shown in Fig. 1f for all mono and hybrid nanofluids used as coolant flowing through the CMPFs heat sink by keeping the water as a reference coolant. The higher value of *PEC* is observed in the case of nanofluids, and the highest enhancement of 57 % and 56 % is obtained at Δp of 1120 Pa and 2280 Pa, respectively, in case of GNP nanoparticles dispersed mono nanofluid compared to the water-cooled CMPFs heat sink. In the case MgO nanoparticles dispersed mono nanofluid, the *PEC* is less than unity at lower $\Delta p = 570$ Pa or inlet velocity flow rate because of slightly lower heat transfer and high pumping power.

The results shown in Fig. 3, reveal that there is not a huge significance in hydraulic thermal performance of mono and hybrid nanofluid having constant volume fraction flowing through the CMPFs heat sink at varying Δp . The results of R_{th} , Nu_{avg} , and *PEC* reveal that GNP dispersed mono nanofluid has the lowest thermal resistance, higher convective heat transfer performance exhibiting highest Nu_{avg} and optimum *PP*. Furthermore, it is suggested to flow the nanofluids at lower *PP* resulting in lower flow velocity.

Further the hydraulic thermal performance is explored by considering only GNP dispersed mono nanofluid by varying the volume fraction (ϕ) from 0 % to 1 % of GNP because GNP-based mono nanofluid exhibited the better cooling performance among other mono and hybrid nanoparticles at varying Δp across the inlet and outlet. It can be seen from Fig. 4a that with the increase of GNP volume fraction, the R_{th} decreases, as expected. The decrease in thermal resistance (R_{th}) is achieved of 32.82 %, 37.0 %, 39.25%, and 41.0 % at ϕ of 0.25 %, 0.50 %, 0.75 %, and 1.0 %, respectively, at $\Delta p = 570$ Pa. In a similar manner, the reduction of 37.1 %, 41.22 %, 43.24 %, and 45.27 % at $\phi = 0.25$ %, 0.50 %, 0.75 %, and 1.0 %, respectively, is achieved in R_{th} at $\Delta p = 2760$ Pa.

The heat transfer enhancement in terms of average Nusselt number (Nu_{avg}) as a function of Δp is presented in Fig. 4b for all cases of ϕ . The

Nu_{avg} increases with the increase of ϕ which shows that addition of nanoparticles augments the heat transfer. Apart from the higher thermal conductivity of nanoparticles, there are some other factors such as thermal-viscous boundary layer, specific heat transfer enhancement mechanisms, Brownian motion of nanoparticles, thermophoresis and molecular interactions of two different types of nanoparticles in the case of hybrid nanoparticles dispersed hybrid nanofluids with base fluid [37, 40] which are not considered and captured in this study.

The increasing trend in volumetric flow rate (Q) and pumping power (*PP*) is obtained by changing the Δp from 570 Pa to 2760 Pa, as shown in Fig. 4c and Fig. 4d, respectively. Moreover, there is no significant variations observed with the change of ϕ from 0 % to 1 % of GNP nanoparticles. The maximum enhancement in Q and *PP* is obtained at 1.15 % and 1.05 %, respectively, at $\phi = 0.25$ % and $\Delta p = 1470$ Pa compared to the $\phi = 0$ %. However, there is no significant enhancement in Q and *PP* observed by the addition of more quantity of nanoparticles.

The combined effect of supplied input power (\dot{Q}) and pumping power (*PP*) is illustrated in Fig. 4e in terms of overall performance (*OP*) as a function of Δp and it can be seen that *OP* decreases exponentially with the increase of Δp as a consequence of higher *PP* at a constant \dot{Q} . Similar to Q and *PP*, there is no significant variation observed in *OP* of varying ϕ . A maximum decrease of 1.24 % is achieved at $\Delta p = 1120$ Pa and $\phi = 1.0$ % compared to the $\phi = 0$ %.

The comparison of performance evaluation criteria (*PEC*) of all selected ϕ of GNP nanoparticles dispersed mono nanofluid cooled CMPFs heat sink is presented in Fig. 4f. It is revealed that the *PEC* increases from $\phi = 0.25$ % to 0.75 %, however it decreases at 1.0 % especially at lower pressure boundary conditions or velocity flow rates. The maximum enhancement in *PEC* is achieved of 60 % for ϕ of 0.50 % and 0.75 % for both Δp of 1120 Pa and 1470 Pa. At higher Δp from 1850 Pa to 2760 Pa, the *PEC* is slightly dropped by about 1–3 % as a consequence of higher *PP*. It is also suggested the increasing the loading of nanoparticles in base fluid decreases the hydraulic, and thermal performance of nanofluid-cooled heat sinks.

The fluid flow dynamics and temperature profile are shown in

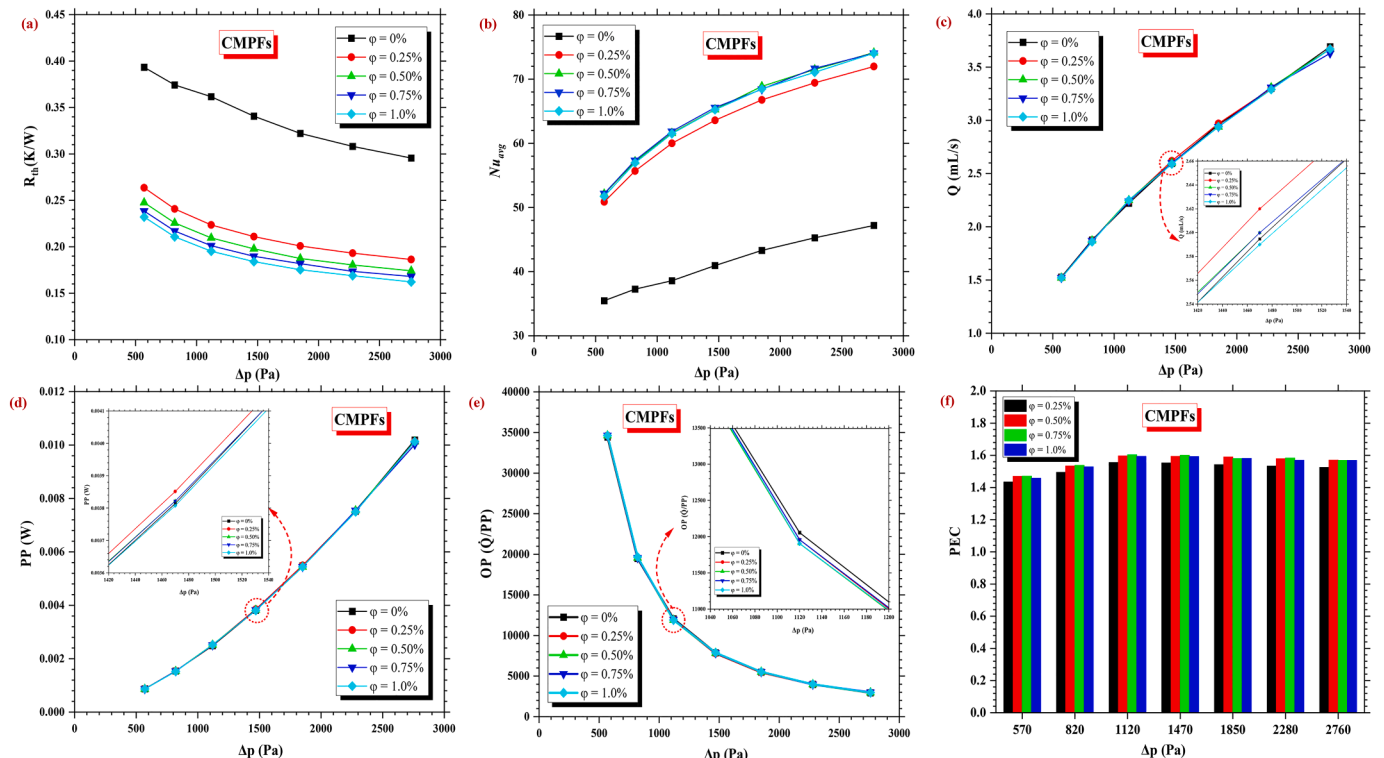


Fig. 4. Variation of (a) R_{th} , (b) Nu_{avg} , (c) Q , (d) *PP*, (e) *OP*, and (f) *PEC* with GNP dispersed mono nanofluid cooled CMPFs heat sink.

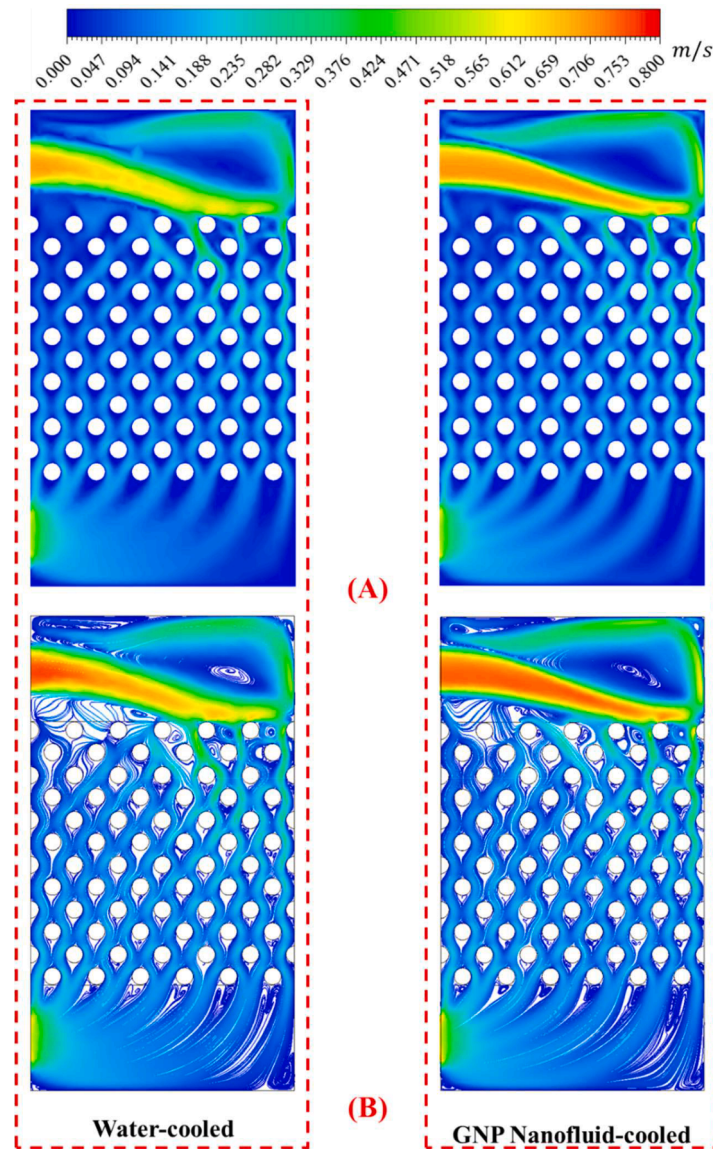


Fig. 5. (A) Velocity contours and (B) Velocity streamlines distribution of water-cooled and $\phi = 1.0\%$ of GNP nanofluid-cooled CMPFs heat sink at $\Delta p = 570$ Pa.

Figs. 5–7. Fig. 5a and b represents the velocity contours and streamline flow, respectively, along the x - y plane by considering $\phi = 1.0\%$ of GNP nanofluid-cooled and water-cooled CMPFs under a Δp of 570 Pa. A large recirculation zone is observed at the top right corner of the inlet header, while a smaller zone forms along the bottom left corner before the flow moves through the pin-fin wetted area. It is important to clarify that these flow recirculation zones are primarily driven by the geometry and flow dynamics within the header. The resulting velocity field then influences the local heat transfer distribution, as areas with recirculating or stagnating flow typically exhibit different heat transfer characteristics compared to regions with streamlined flow. Therefore, while the heat transfer distribution is a consequence of the velocity field, the velocity field itself is not directly influenced by the heat transfer process. The large circulation region at the left top side reduces the flow velocity of the fluid upstream of the fins and also generates the small recirculation of flow left bottom side which encompasses the fluid velocity. The fluid flow from upstream to the downstream shows a relatively uniform distribution governed by the smooth, uniform configuration of circular pin-fins. At the downstream surface of fins, flow experiences the separation because of this wake formation occurs at the rear side of the fins. This generation of wakes at the rear side of the fins diverts the flow field and

forms the vortices, and as a consequence, this augments the fluid mixing, secondary flow, and turbulence at the rear of the fins [18,40]. It is observed from Fig. 5a and Fig. 5b that flow field in both cases are very much similar which is also reflected from the quantitative results of pumping power and volumetric flow rate, shown in Fig. 3c and Fig. 3d, respectively. In both cases, higher velocities exhibit in the inlet header side, with noticeable recirculation zones and flow separations near the inlet, indicating inefficient flow distribution. The streamlines of both coolants show complex and turbulent flow patterns with prominent recirculation zones and vortices, accelerating effective heat transfer depending on the type of coolant, i.e. water or GNP nanofluid, in present study. These observations validate the findings from Fig. 2, where accurate flow rate predictions and acceptable thermal resistance values were reported for varying pressure drops.

Fig. 6 illustrates the temperature distribution across the x - y and x - z planes for both water-cooled and GNP nanofluid-cooled, having ϕ of 1.0% of GNP nanoparticles, CMPFs heat sinks at a Δp of 570 Pa. The temperature gradient is highest from the upstream to the downstream. The temperature zone is high downstream as nanofluid flows through the fins which illustrates the optimal heat transfer. Similarly, the temperature gradient change from the bottom to the top of the heat sink.

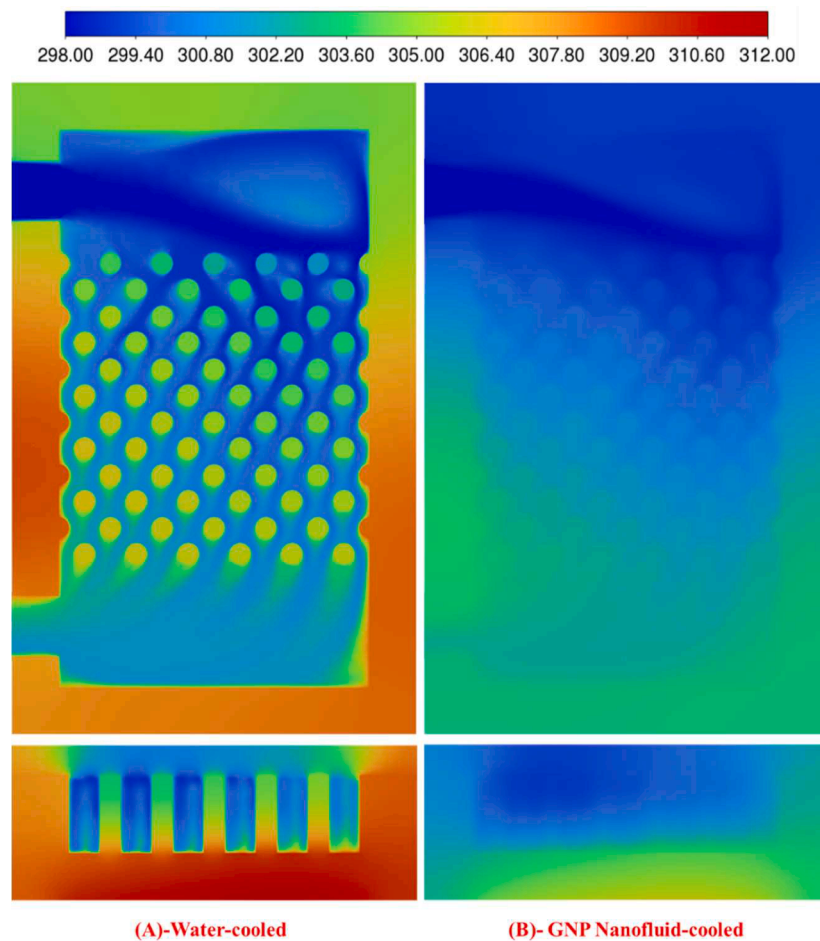


Fig. 6. Temperature distribution of x-y and x-z planes for (a) water-cooled and (b) $\phi = 1.0\%$ of GNP nanofluid-cooled CMPFs heat sink at $\Delta p = 570$ Pa.

The temperature gradient is higher at the bottom of the heat sink and around the fins, increasing from the upstream to the downstream. The temperature gradient across the heat sink surface is noticeably lower, due to the reduced temperature range, in case of GNP nanofluid-cooled heat sink, indicating enhanced heat transfer capabilities due to the higher thermal conductivity of the GNP nanoparticles. Whereas, in case of water-cooled heat sink exhibits high-temperature localization at the fins, indicating lower heat transfer values. This enhanced heat transfer is supported by Fig. 3a, which shows a significant reduction in thermal resistance (R_{th}) for the GNP nanofluid compared to water, and by Fig. 3b, which depicts a higher average Nusselt number (Nu_{avg}) for the nanofluid. The enhancement in heat transfer is expected that GNP-nanofluid can maintain the fins and the heated base at a lower temperature, which is noticeable in the Fig. 6b. The performance evaluation criterion (PEC) results, shown in Fig. 3f, further quantifies the superior cooling performance of the GNP nanofluid under varying Δp . The augmentation of heat transfer is higher when compared to the water-cooled because of the dispersion of nanoparticles, which exhibit the enhanced surface area with the interaction between particle-particle and particle-liquid phases [37,40,45–47].

A qualitative analysis of temperature field and velocity streamlines flow field cumulatively is illustrated in Fig. 7 as an isometric view of CMPFs heat sink for (a) water-cooled and (b) GNP nanofluid-cooled, having ϕ of 1.0 % of GNP nanoparticles at $\Delta p = 570$ Pa. The three-dimensional view of both cases reflects the real-time picture of flow regime and temperature distribution across the heat sink surfaces with effect of water and GNP dispersed nanofluid as coolants. The comparison between water-cooled and GNP nanofluid-cooled CMPFs heat sink highlights the superior cooling performance of the GNP nanofluid in

terms of reduced temperature distribution. This uniform temperature distribution, indicating efficient heat dissipation, is because of higher thermal conductivity exhibiting GNP nanofluid with uniformly flow field at a certain pressure boundary conditions. The smoother flow pattern improves heat transfer performance which can be observed with the data presented in Fig. 3a and b, where the R_{th} is significantly reduced, and the Nu_{avg} is increased for the GNP nanofluid compared to water. In contrast, the water-cooled heat sink, shown in Fig. 7a, presents higher temperature localization around the fins, signifying lower heat transfer efficiency. In summary, the combined data from the results clearly demonstrate that GNP nanofluid significantly enhances the thermal management capabilities of CMPFs heat sinks compared to water, corroborating the study's conclusion that GNP nanofluid is more effective in improving the overall performance of these cooling systems.

4. Conclusion

The current numerical study presents the heat and fluid flow phenomenon of Ag, MgO, GNP and MWCNT dispersed mono and hybrid water-based nanofluid-cooled circular micro pin-fins (CMPFs) heat sink at varying volume fraction (ϕ) and pressure drop (Δp). The results revealed that the addition of Ag, MgO, GNP and MWCNT nanoparticles in base fluid enhance the heat transfer rate. The higher average Nusselt number (Nu_{avg}) and lower thermal resistance (R_{th}) are achieved with the increase of Δp . The highest Nu_{avg} and lowest R_{th} are obtained with GNP added water-based nanofluid because of the higher thermal conductivity of GNP nanoparticles.

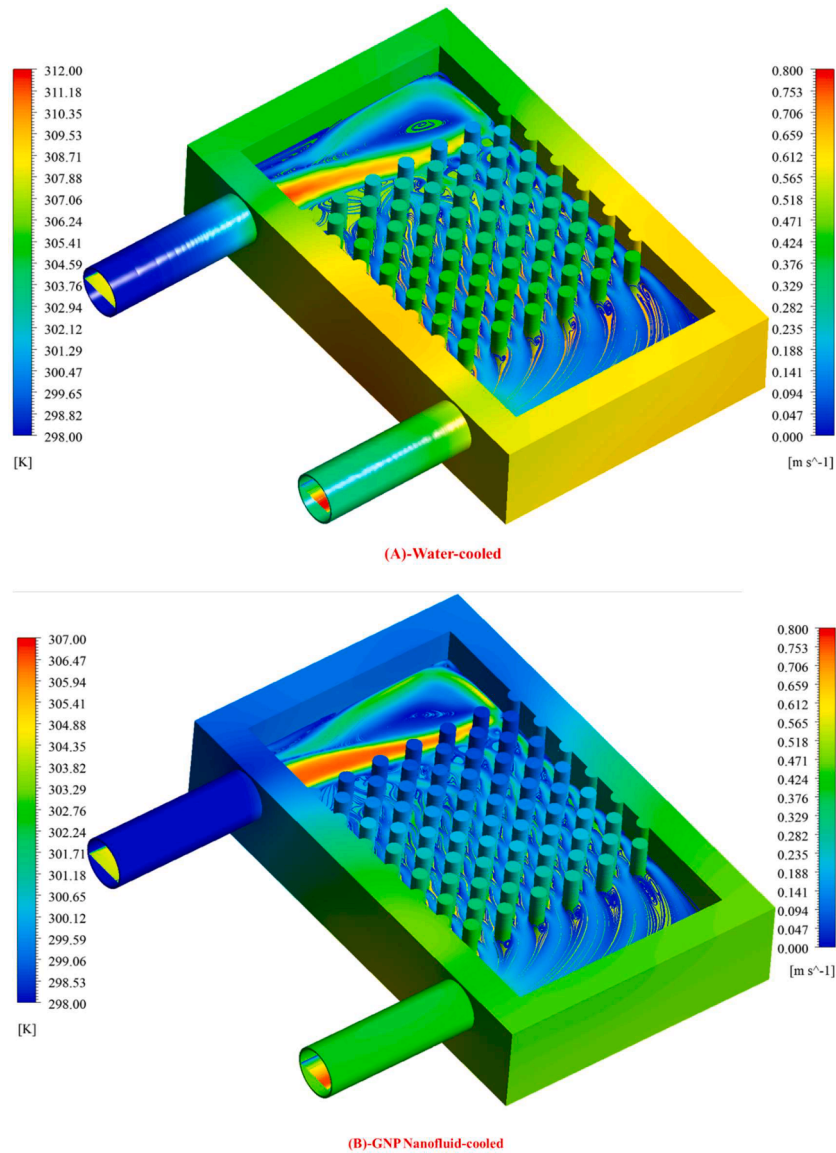


Fig. 7. Temperature and velocity streamlines distribution of (A) water-cooled and (B) $\phi = 1.0\%$ of GNP nanofluid cooled CMPFs heat sink at $\Delta p = 570$ Pa.

- The results revealed that the addition of Ag, MgO, Ag-MgO, GNP, MWCNT, and GNP-MWCNT nanoparticles enhance the h_{avg} , Nu_{avg} and reduce the R_{th} in case of circular and rectangular micro pin-fins cases with the increase of Δp .
- At $\Delta p = 570\text{Pa}$ and $\phi = 1\%$, the reductions of 25.20 % and 40.71 % in R_{th} are attained with Ag and GNP, respectively, nanoparticles dispersed mono nanofluids compared to the water-cooled CMPFs heat sink.
- The enhancement in Nu_{avg} is achieved of 45.06 % and 54.26 % at Δp of 570 Pa and 2760 Pa, respectively, in case of GNP-dispersed mono nanofluid compared to the water-cooled CMPFs heat sink.
- The higher value of performance evaluation criteria (PEC) is observed in the case of nanofluids and the highest enhancement of 57 % and 56 % is obtained at Δp of 1120 Pa and 2280 Pa, respectively, in case of GNP nanoparticles dispersed mono nanofluid compared to the water-cooled CMPFs heat sink.
- The pumping power (PP) and volumetric flow rate (Q) are increased; however, the overall performance (OP) is exponentially decreased with an increase of Δp from 570Pa to 2760Pa.
- The PEC increases from $\phi = 0.25\%$ to 0.75 %. However, it decreases at 1.0 %, especially at lower pressure boundary conditions or velocity flow rates. The maximum enhancement in PEC is achieved of 60 % for ϕ of 0.50 % and 0.75 % for both Δp of 1120 Pa and 1470 Pa. At higher Δp from 1850 Pa to 2760 Pa, the PEC is slightly dropped by about 1–3 % as a consequence of higher PP .
- The loading of nanoparticles in the base fluid significantly enhances the thermohydraulic performance of nanofluid-cooled heat sinks. This improvement is primarily due to the substantial reduction in thermal resistance, which exceeds one third, without a significant increase in friction losses. Consequently, the electronic components can operate at lower temperatures with the same pumping power, leading to a more efficient and reliable cooling system.
- While the incorporation of mono and hybrid nanofluids at a constant volume fraction into the CMPFs heat sink does not lead to a significant change in hydraulic performance across varying Δp , it does notably enhance the thermal performance. Specifically, the results indicate that the GNP dispersed mono nanofluid provides the lowest R_{th} , the highest Nu_{avg} , and optimal PP among the tested configurations. These findings demonstrate that the use of GNP dispersed mono nanofluid in a staggered arrangement significantly improves the convective heat transfer performance, thereby enhancing the overall thermal performance of the nanofluid-cooled heat sink.

CRedit authorship contribution statement

Adeel Arshad: Writing – original draft, Visualization, Validation, Software, Methodology, Investigation, Formal analysis, Data curation, Conceptualization. **Muhammad Ikhtlaq:** Writing – review & editing, Software, Methodology. **Muhammad Saeed:** Writing – review & editing, Visualization. **Muhammad Imran:** Writing – review & editing, Supervision, Resources, Project administration, Visualization.

Declaration of competing interest

The authors declare that they have no known competing financial interests or personal relationships that could have appeared to influence the work reported in this paper.

Data availability

The authors do not have permission to share data.

Acknowledgments

This research is facilitated by the Faculty of Environment, Science and Economy, University of Exeter, United Kingdom and Department of Mechanical, Biomedical and Design Engineering, Aston University, Birmingham, United Kingdom research infrastructures. *“For the purpose of open access, the author has applied a Creative Commons Attribution (CC BY) licence to any Author Accepted Manuscript version arising from this submission.”*

References

- [1] M. Azarifar, M. Arik, J.Y. Chang, Liquid cooling of data centers: a necessity facing challenges, *Appl. Therm. Eng.* 247 (2024) 123112.
- [2] M. Ohring, L. Kasprzak, *Reliability and Failure of Electronic Materials and Devices*, Academic Press, 2014.
- [3] M. Saeed, M.H. Kim, Numerical study on thermal hydraulic performance of water cooled mini-channel heat sinks, *Int. J. Refrig.* 69 (2016) 147–164.
- [4] M. Saeed, M.H. Kim, Header design approaches for mini-channel heatsinks using analytical and numerical methods, *Appl. Therm. Eng.* 110 (2017) 1500–1510.
- [5] W. Duangthongsuk, S. Wongwises, A comparison of the heat transfer performance and pressure drop of nanofluid-cooled heat sinks with different miniature pin fin configurations, *Exp. Therm. Fluid Sci.* 69 (2015) 111–118.
- [6] A. Karimipour, A. D’Orazio, M.S. Shadloo, The effects of different nano particles of Al_2O_3 and Ag on the MHD nano fluid flow and heat transfer in a microchannel including slip velocity and temperature jump, *Phys. E Low Dimens. Syst. Nanostruct.* 86 (2017) 146–153.
- [7] M. Saeed, M.H. Kim, Heat transfer enhancement using nanofluids (Al_2O_3 - H_2O) in mini-channel heatsinks, *Int. J. Heat Mass Transf.* 120 (2018) 671–682.
- [8] L. Shi, et al., Thermo-physical properties prediction of carbon-based magnetic nanofluids based on an artificial neural network, *Renew. Sustain. Energy Rev.* 149 (2021) 111341.
- [9] A. Arshad, et al., A review on graphene based nanofluids: preparation, characterization and applications, *J. Mol. Liq.* 279 (2019) 444–484.
- [10] M. Saeed, et al., Numerical investigation of the thermohydraulic characteristics of microchannel heat sinks using supercritical CO_2 as a coolant, *J. Supercrit. Fluids* 176 (2021) 105306.
- [11] A.A. Awais, M. Saeed, M.H. Kim, Performance enhancement in minichannel heat sinks using supercritical carbon dioxide (sCO_2) as a coolant, *Int. J. Heat Mass Transf.* 177 (2021) 121539.
- [12] M. Afrand, Experimental study on thermal conductivity of ethylene glycol containing hybrid nano-additives and development of a new correlation, *Appl. Therm. Eng.* 110 (2017) 1111–1119.
- [13] A. Dey, Z.U. Ahmed, M.R. Alam, Thermal and exergy analysis of Pin-finned heatsinks for nanofluid cooled high concentrated photovoltaic thermal (HCPV/T) hybrid systems, *Energy Convers. Manag.* X 16 (2022) 100324.
- [14] M.U. Sajid, H.M. Ali, Recent advances in application of nanofluids in heat transfer devices: a critical review, *Renew. Sustain. Energy Rev.* 103 (2019) 556–592.
- [15] J. Wang, et al., A review on nanofluid stability: preparation and application, *Renew. Sustain. Energy Rev.* 188 (2023) 113854.
- [16] S. Yan, et al., Using artificial intelligence and two-phase numerical simulation method for investigating the effect of the shape of pin fins on the entropy production of nanofluid flow in a heatsink at different flow rates, *Eng. Anal. Bound. Elem.* 155 (2023) 1168–1176.
- [17] T. Ambreen, A. Saleem, C.W. Park, Numerical analysis of the heat transfer and fluid flow characteristics of a nanofluid-cooled micropin-fin heat sink using the Eulerian-Lagrangian approach, *Powder Technol.* 345 (2019) 509–520.
- [18] T. Ambreen, et al., Performance analysis of hybrid nanofluid in a heat sink equipped with sharp and streamlined micro pin-fins, *Powder Technol.* 355 (2019) 552–563.
- [19] A. Shahsavari, et al., Extensive investigation of the fluid inlet/outlet position effects on the performance of micro pin-fin heatsink through simulation, *Energy Sources Part A Recov. Util. Environ. Eff.* 44 (4) (2022) 9489–9505.
- [20] A. Shahsavari, P. Farhadi, I.B. Askari, Numerical investigation of the effect of perforation inclination angle on the performance of a perforated pin-fin heatsink using two-phase mixture model, *Eng. Anal. Bound. Elem.* 156 (2023) 488–498.
- [21] D. Wang, T. Hai, The parametric optimization to enhance the pin-fin microchannel heatsink performance using splitter and water/silver nanofluid applying the two phase mixture model, *Eng. Anal. Bound. Elem.* 146 (2023) 216–225.
- [22] A. Shahsavari, O. Yari, I.B. Askari, The entropy generation analysis of forward and backward laminar water flow in a plate-pin-fin heatsink considering three different splitters, *Int. Commun. Heat Mass Transf.* 120 (2021) 105026.
- [23] H. Ghazizadeh-Ahsaei, et al., The parametric optimization of a pin-fin heatsink in the presence of ultrasonic vibration based on the second law of thermodynamic, *Chem. Eng. Process. Process Intensif.* 193 (2023) 109525.
- [24] H. Ghazizadeh-Ahsaei, et al., The effect of inlet velocity profile on entropy generation and hydrothermal performance of a pin-fin heatsink with biologically prepared silver/water nanofluid coolant: two-phase mixture model, *Eng. Anal. Bound. Elem.* 150 (2023) 309–317.
- [25] C. Zhu, et al., Numerical simulation and optimization with artificial neural network of two-phase nanofluid flow in a circular heatsink with cylindrical pin-fins, *Eng. Anal. Bound. Elem.* 148 (2023) 305–316.
- [26] M.R. Haque, et al., Numerical investigation of heat transfer performance for rectangular, elliptical, and airfoil shaped pin fin heatsinks through the novel combination of perforation and bulge inserts, *Int. Commun. Heat Mass Transf.* 138 (2022) 106352.
- [27] S. Sadrabadi Haghighi, H.R. Goshayeshi, I. Zahmatkesh, Experimental investigation of forced convection heat transfer for different models of PPFHS heatsinks with different fin-pin spacing, *Heliyon* 10 (1) (2024), <https://doi.org/10.1016/j.heliyon.2023.e23373>.
- [28] D. Wang, T. Hai, Entropy analysis and parametric optimization on the Nano fluid flow and heat transfer of a pin-fin heatsink with the splitter using the two-phase mixture model, *Eng. Anal. Bound. Elem.* 146 (2023) 997–1006.
- [29] J. Liu, et al., Artificial intelligence-based entropy generation investigation of two-phase nanofluid flow in a heatsink with pin fins, *Eng. Anal. Bound. Elem.* 155 (2023) 212–225.
- [30] M. Harris, et al., Heat transfer optimisation using novel biomorphic pin-fin heat sinks: an integrated approach via design for manufacturing, numerical simulation, and machine learning, *Therm. Sci. Eng. Prog.* 51 (2024) 102606.
- [31] T. Hai, et al., The entropy generation analysis of a pin-fin heatsink with Fe_3O_4 ferrofluid coolant and considering four different pin-fin shapes (circular, square, rhombus, and triangular) in the presence of the magnetic field, *J. Magn. Magn. Mater.* 580 (2023) 170904.
- [32] H. Babar, et al., Staggered oriented airfoil shaped pin-fin heat sink: investigating the efficacy of novel water based ferric oxide-silica hybrid nanofluid, *Int. J. Heat Mass Transf.* 194 (2022) 123085.
- [33] P. Bhandari, et al., Design modifications in micro pin fin configuration of microchannel heat sink for single phase liquid flow: a review, *J. Energy Storage* 66 (2023) 107548.
- [34] A. González, E. Ruz, E. Castillo, Numerical study of the fluid dynamics and heat transfer for shear-thinning nanofluids in a micro pin-fin heat sink, *Case Stud. Therm. Eng.* 28 (2021) 101635.
- [35] M. Manninen, V. Taivassalo, S. Kallio, On the mixture model for multiphase flow, *Finland* (1996), 1997-12-31.
- [36] L. Schiller, A drag coefficient correlation, *Zeit. Ver. Deutsch. Ing.* 77 (1933) 318–320.
- [37] O. Mahian, et al., Recent advances in modeling and simulation of nanofluid flows—Part I: fundamentals and theory, *Phys. Rep.* 790 (2019) 1–48.
- [38] O. Mahian, et al., Recent advances in modeling and simulation of nanofluid flows—Part II: applications, *Phys. Rep.* 791 (2019) 1–59.
- [39] H.M. Ali, A. Arshad, Experimental investigation of n-icosane based circular pin-fin heat sinks for passive cooling of electronic devices, *Int. J. Heat Mass Transf.* 112 (2017) 649–661.
- [40] Z. Said, et al., Recent advances on the fundamental physical phenomena behind stability, dynamic motion, thermophysical properties, heat transport, applications, and challenges of nanofluids, *Phys. Rep.* 946 (2022) 1–94.
- [41] H. Babar, et al., The promise of nanofluids: a bibliometric journey through advanced heat transfer fluids in heat exchanger tubes, *Adv. Colloid Interface Sci.* 325 (2024) 103112.
- [42] A. Shahsavari, et al., On the cooling performance and entropy generation characteristics of a heat sink under ultrasonic vibration: exploring the impact of porous medium, *Int. J. Heat Mass Transf.* 215 (2023) 124500.
- [43] M. Ikhtlaq, Y.M. Al-Abdali, M. Khiadani, Nozzle exit conditions and the heat transfer in non-swirling and weakly swirling turbulent impinging jets, *Heat Mass Transf.* 56 (2020) 269–290.
- [44] H.C. Chiu, et al., The heat transfer characteristics of liquid cooling heat sink with micro pin fins, *Int. Commun. Heat Mass Transf.* 86 (2017) 174–180.

- [45] A. Arshad, et al., Thermophysical characteristics and enhancement analysis of carbon-additives phase change mono and hybrid materials for thermal management of electronic devices, *J. Energy Storage* 34 (2021) 102231.
- [46] B.X. Wang, L.P. Zhou, X.F. Peng, Surface and size effects on the specific heat capacity of nanoparticles, *Int. J. Thermophys.* 27 (1) (2006) 139–151.
- [47] L. Wang, et al., Enhancement of molar heat capacity of nanostructured Al_2O_3 , *J. Nanopart. Res.* 3 (5) (2001) 483–487.